Effects of high intensity neutron flux on in-situ spin-exchange optical pumping of ^{3}He

E Babcock[1*]**, S Boag**[2]**, C Beecham**[2]**, T E Chupp**[3]**, T R Gentile**[4]**, G L Jones**[5]**, A K Petukhov**[6] **and T G Walker**[7]

[1]Jülich Centre for Neutron Science, Institut für Festkörperforshung, Forschungszentrum Jülich GmbH, 85747 Garching, Germany

[2] ISIS, Chilton, Didcot OX11 QX United Kingdom

[3] University of Michigan, Ann Arbour MI 48109 USA

[4] National Institute of Standards and Technology, Gaithersburg MD 20899 USA

[5] Hamilton College, Clinton NY 13323 USA

[6] Institut Laue Langevin, 38042 Grenoble France

[7] University of Wisconsin Madison, Madison WI 55106 USA

E-mail: `e.babcock@fz-juelich.de`

Abstract. Prior studies revealed neutron beam-induced alkali-metal spin relaxation in ^{3}He cells polarized in-situ by spin-exchange optical pumping. These effects are minor for neutron beams of low to moderate intensity, but become important at the highest neutron flux levels available in the full spectrum beams of high flux neutron sources. It was found that the relaxation consisted of a fast and a slow component, but the origin of neither is understood. This work further explored the mechanisms of this effect by measuring the magnitude and time dependence of alkali-metal spin-relaxation rates as a function of N_2 and ^{3}He composition. The experiments were performed on a thermal neutron beam line at the Institut Laue-Langevin with a maximum neutron flux of 2.4×10^9 cm^{-2} s^{-1}.

1. Introduction

Polarized ^{3}He has applications in many areas of neutron science as a neutron polarizer or polarization analyzer as neutron spin filter cells (NSF) [1, 2]. While typically the metastability exchange optical pumping method (MEOP) [3] can produce more polarized ^{3}He, up to 1 bar-liter to 2 bar-liters per hour [1], current methods with spin-exchange optical pumping (SEOP) can also provide high production rates. Methods such as frequency narrowed diode array bars [4, 5] and hybrid SEOP [6] have led to increased performance and speed for this method such that cells containing more than 1 bar-liter to 2 bar-liters of gas can be polarized in 1 day time scales [7, 8]. Additionally both methods have achieved ^{3}He polarizations of 80% with neutron measurements [1, 9, 10]. However the ^{3}He is often polarized in a laboratory away from the neutron instrument and thus undergoes polarization decay with typical time constants on neutron instruments of 100 hours to 300 hours.

In-situ optical pumping is one way to counteract the effects of the polarization decay of the ^{3}He and potentially improve time averaged neutron performance and ^{3}He polarization. True in-situ optical pumping to maintain steady ^{3}He polarization can currently only be done with the SEOP method as it can be performed at the ^{3}He pressures required for use as a neutron spin
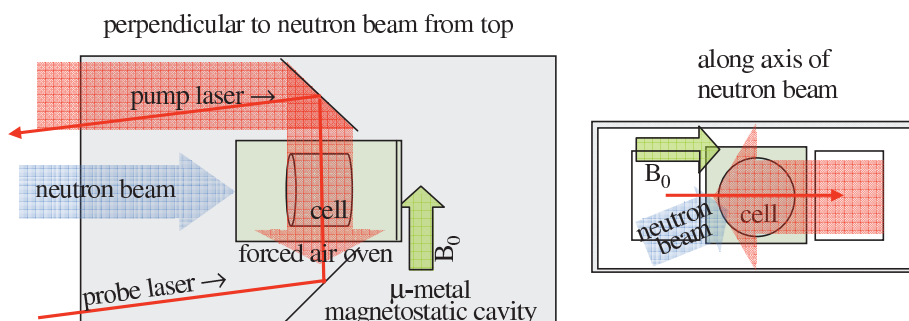
Figure 1. The spin-exchange optical pumping setup used for this experiment. One pump laser was used which counter propagated with the probe laser.

filter. However previous studies performed by members of this team, on the fundamental neutron physics beam line PF1B at the Institut Laue-Langevin (ILL)[11], had shown adverse effects to the performance of the optical pumping process in conditions of extreme levels of neutron flux which are currently normally only experienced in cold neutron particle physics beams. With increased instrument neutron flux due to ever improving neutron optics and higher intensity neutron sources, the effects could eventually be relevant to developing ^{3}He spin filters for such new instrumentation.

The reduced optical pumping performance is caused by increased alkali-metal relaxation rates which in turn increases the amount of required laser power. In extreme cases this leads to lowered alkali-metal polarization and thus lowered ^{3}He polarization. In high flux conditions this increase in alkali metal relaxation was measured vs neutron flux from 4×10^7 s^{-1} cm^{-2} to 5×10^9 s^{-1} cm^{-2} for a cold neutron spectrum (i.e. mean neutron wavelength 0.45 nm) and appeared to follow a square root of flux dependence [12]. The exact cause of the effect was not understood and it is further complicated by the fact that the effect was found not only to depend on neutron flux, but it also appeared to have two relevant time scales, one affecting the alkali metal relaxation quickly, in less than a second, and the other affecting it on time scales on the order of hundreds of seconds. Additionally, the alkali-metal relaxation seemed to depend on the amount of nitrogen buffer gas in the cell. Nitrogen, which must be present in SEOP cells to prevent radiation trapping, while probably preventing effects of ionization on direct ^{3}He nuclear spin relaxation as was observed in particle beam experiments [13, 14], seemed to be increasing the magnitude of the alkali-metal spin-relaxation for the neutron beam case. Consequently, additional measurements were conducted in order to explore the the nature of the two time constants observed in the first experiments and also the nitrogen pressure dependence of the effect.

2. Experiment
The same apparatus as in Ref. [15] was installed on the tomography beam line at the ILL and is shown in Fig. 1. This beam employs thermal neutrons with an assumed mean neutron wavelength of 0.18 nm and a particle flux of 2.4×10^9 s^{-1} cm^{-2}. The flux was calibrated using the gold foil activation method and was a constant intensity over the duration of the experiment. The neutron flux could not be varied in a calibrated way to do flux dependent tests. Since this beam has a different mean neutron wavelength than in [12] it has a different fractional neutron absorption for a given cell and has roughly half the absolute particle flux of the beam used in that prior work. For confirmation, the cell Lucky Luke was used in both experiments and gave a reasonable agreement in the measured effect when corrections for the differences in the two beams are made, despite the very different characteristics.
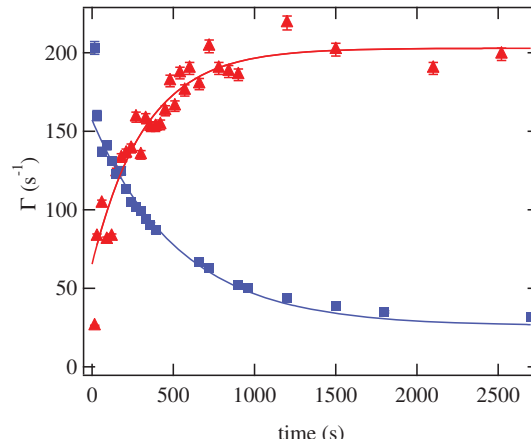
Figure 2. A sample of the measured alkali-metal relaxation rates, Γ, as a function of time after the beam was opened, red triangles, or closed, blue squares, for the cell Tin Man.

The alkali-metal relaxation was measured in the same way as in Ref. [12] using a method referred to as relaxation in the dark [16]. A diagram of the apparatus is shown in Fig. 1. The alkali-metal was polarized to low polarization by the optical pumping laser running at low power and at a wavelength a few nanometers away from the Rb resonance. A low power linearly polarized probe laser tuned to 778 nm was then used to observe the Faraday rotation, which is proportional to the Rb polarization for constant Rb density, while the pump laser was chopped at about 1 Hz to observe the decay transients of the Rb polarization. The alkali-metal relaxation was in this way measured as a function of time after the beam was opened or closed. In this paper we will always report the measured alkali-metal relaxation rates, which are a factor of the slowing down factor lower than the actual electronic relaxation rates which are proportional to the photon demand to polarize the vapor [17]. A sample of data is shown in Fig. 2. In this way we were able to extract the fraction of the effect that happened quickly at t=0, and the fraction that happened with a long time constant from the t=0 intercepts of exponential fits to the data.

The tomography beam had a "fast shutter" that could be used to block the neutron beam (but not the epi-thermal components of the spectrum which are not absorbed by the ^{3}He cell anyway) on the time scale of less than one second. From observing the response of the Faraday rotation signal while this shutter was pulsed, it appeared that the quick change in the alkali-metal polarization was coincident with the opening and closing of this shutter, verifying previous observations [12], but with more confidence.

For these measurements 4 cells were used, 3 permanently sealed cells of different ^{3}He and N_2 gas compositions and one valved cell that allowed us to vary the ^{3}He and N_2 partial pressures. The parameters of the cells and the different fillings for the valved cell are given in Table 1. Most of the relaxation measurement data was taken at a temperature of 170 °C as measured by a thermocouple placed near the cell. For the Lucky Luke cell data was also taken at 150 °C and 190 °C. The 190 °C data had a higher zero flux alkali-metal relaxation in agreement with the known temperature dependence of the relaxation cross sections for the gas composition of the cell. The change in measured alkali-metal relaxation showed the same magnitude and it had the same fraction of slow and fast components as the 170 °C data within uncertainties. The 150 °C data is more complex. The measured alkali-metal relaxation when exposed to the neutron flux for the first time rose from 15 s^{-1} to 126 s^{-1}, in rough agreement with the 170 °C and 190 °C data for the total change in alkali-metal relaxation. The initial zero flux relaxation rate of 15 s^{-1} before exposure to the neutron flux was again in agreement with the known cross sections

cell name	[^{3}He](bar)	[N_2](bar)	L_1 (cm)	L_3 (cm)	A_n	$\Delta\Gamma$ (1/s)$\pm$5%
Lucky Luke	0.5	0.1	5.0	1.6	0.33	100
Tin Man	0.5	0.4	2.0	0.6	0.28	176
Scarecrow	0.5	0.02*	8.4	3.0	0.28	36
valved cell	0.64	0.12	4.0	1.3	0.34	141
	0.90	0.02	5.1	1.8	0.45	119
	2.4	0.05	1.9	0.7	0.79	296
	2.2	0.4	1.2	0.4	0.77	354
	0	2.0	0.5	0.1	0	0
	1.4	0	3.6	1.4	0.60	96
	0.4	0	12.8	4.8	0.23	58

Table 1. List of cells and their parameters used in this experiment. All the cells were 5 cm by 5 cm cylinders except for Lucky Luke which is a 6 cm by 6 cm cylinder. The * on the [N_2] value is to denote this parameter is not well known due to the factors at the time of the cell filling. All of the cells contained Rb only for alkali-metal. L_1 is the stopping length of proton created by a neutron absorption and L_3 is the triton stopping length. A_n is the fraction of absorbed neutron flux assuming a thermal Boltzmann distribution with 0.18 nm peak wavelength. $\Delta\Gamma$ is the total change in measured alkali-metal relaxation. All quantities are assumed accurate to the last digit except for $\Delta\Gamma$ which has a relative standard uncertainty of 5 %. The error bars are determined from the typical uncertainties in the exponential fits to the alkali-metal relaxation vs time such as those shown in Fig. 2.

for the cells gas composition and temperature. However after 2000 s with the beam off, the new zero flux relaxation remained higher than expected at 44 s^{-1}.

The time constants for the build up and decay are not necessarily the same. As can be seen in Fig. 2 the time constant for the build up of alkali-metal relaxation after the neutron beam is opened appears to be faster than the decay after the neutron beam is closed. For the data shown in Fig. 2 the time constant was 320 s $\pm$ 50 s for the build up and 550 s $\pm$ 25 s for the decay of neutron induced alkali-metal relaxation. For the valved cell without N_2 the build up of relaxation happened very quickly, reaching its maximum value after perhaps 30 s with the decay having a time constant of 165 s $\pm$ 45 s and 320 s $\pm$ 20 s for the 0.4 bar and 1.4 bar ^{3}He data respectively. Because of this it is more difficult to extract the slow and fast components for the valved cell without N_2 for the build up data. The extracted values of the slow and fast components for the zero N_2 data points are from the decay only which gave reasonable exponential fits. For the other data points the values are the average values obtained from the zero-crossings of the exponential fits to the build up and decay. The relative standard uncertainty for this analysis is 10% of $\Delta\Gamma$ for both the slow and fast component.

The valved cell always had higher alkali-metal relaxation than the sealed cells. Even in the absence of neutron flux the measured alkali-metal relaxation rates were higher than what one would expect from the known relaxation cross sections for the filled gas composition and temperature. This was most likely due to the presence of additional gas impurities from the filling of the cell. This makes it difficult to compare the valved cell directly in absolute terms with the sealed cells. Since the measured alkali-metal relaxation without neutron flux was stable over the course of the experiments and was repeatable, we believe the data can still provide additional qualitative information on the observed effects. However as can be seen in Table 1 it appears that the magnitude of the neutron induced alkali-metal relaxation is higher for cell fillings similar to those of the sealed cells measured, therefore it is likely the unknown impurities are also influencing the neutron induced alkali-metal relaxation mechanisms.
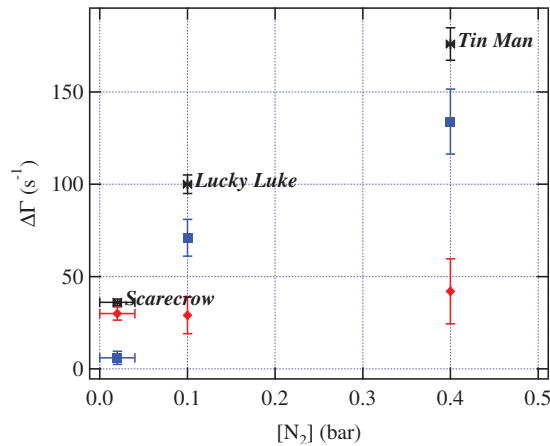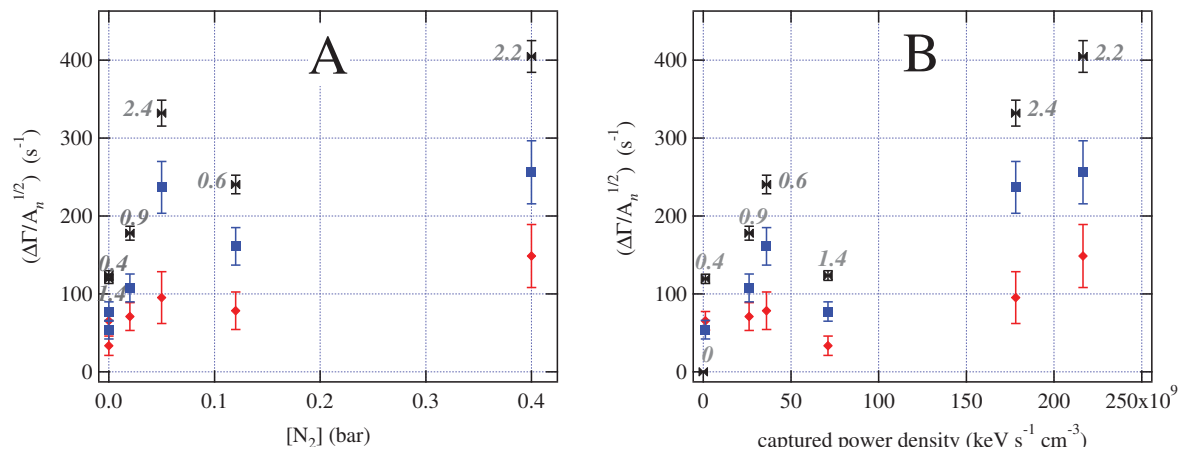
Figure 3. The measured alkali-metal relaxation versus [N$_2$] for the sealed cells. Black bow-ties are the total change in measured alkali-metal relaxation, blue squares are the deduced slow portion, and red diamonds are the deduced fast portion. The x-axis error bars for the Scarecrow cell are included because the value of [N$_2$] for this cell was estimated from it optical pumping properties and has an uncertainty of ± 0.02 bar.

In Fig. 3 the amount of change in alkali-metal relaxation as a function of N$_2$ pressure is plotted for the three sealed cells. As one can see, the slow component is increasing with N$_2$, however the fast proportion is more steady. Ref. [12] showed that the increase in alkali-metal relaxation followed a square root of neutron flux dependence. Here all of the sealed cells measured had similar amounts of captured neutron flux due to their similar ^{3}He densities, thus no corrections for neutron absorption are needed to compare the data from one cell another.

As stated earlier the valved cell data is complicated because of probable gas contamination due to the cell refilling process. This contaminant increased the alkali-metal relaxation rates in the absence of neutron flux by as much as a factor of 2 over what was expected for the measured temperature and gas fill pressures using the known Rb-Rb, Rb-^{3}He and Rb-N$_2$ spin destruction cross sections. Since we do not know the exact origin of the increased relaxation in the valved cell, it is impossible to surmise how it could have affected the relaxation during neutron absorption, and we show this data noting this strong caveat. As a control the valved cell was also filled without ^{3}He, i.e. only N$_2$ buffer gas. Without absorbed neutron flux there was no observed change in alkali-metal relaxation.

The neutron absorption is a function of [^{3}He] where in Ref. [12] the increased alkali-metal relaxation effect was shown to scale as the square root of absorbed neutron flux. Given the range of [^{3}He] values measured for the valved cell, these data should thus be normalized to the square root of the relative neutron absorptions, i.e. by $A_n^{1/2}$, where the values of A_n were given in Table 1. Figure 4A plots the fast and slow components and total $\Delta\Gamma$ normalized by $A_n^{1/2}$ for the valved cell data versus [N$_2$]. One may see that the slow components show a dependence on [N$_2$]. However the data from the 2.4 bar ^{3}He filling seem to contradict the hypothesis that the N$_2$ is mainly responsible for the increase in the magnitude of the effect given this cell had a very low [N$_2$] but high $\Delta\Gamma$.

Perhaps the high $\Delta\Gamma$ for this cell filling is because when [N$_2$] and/or [^{3}He] are changed the energy captured by the gas of the cell is also changing. The absorption of neutrons by the ^{3}He creates charged hydrogen and tritium nuclei which deposit energy as they travel through the cell before either coming to rest in the gas or hitting the cell's wall, where the distance travelled

Figure 4. The measured alkali-metal relaxation versus [N$_2$] (graph A) and captured power density (graph B) for the valved cell with different gas fillings. In both graphs the values of $\Delta\Gamma$ have been normalized by $A_n^{1/2}$ to account for the flux dependence shown in Ref. [12]. Black bow-ties are the total change in alkali-metal relaxation, blue squares are the deduced slow portion, and red diamonds are the deduced fast portion. The numbers labelling the markers denote the ^{3}He pressure of the cell for the particular cell filling as given in Table 1.

inside the cell, and thus energy deposited in the gas, is a function of both [^{3}He] and [N$_2$]. This effect should also be considered in order to compare the valved cell data. Thus we also plot in Fig. 4B $\Delta\Gamma$ normalized by $A_n^{1/2}$ versus captured power density, the calculation of which is described below, for the given gas composition.

The stopping power of a gas target for charged particles is a function of the gases in the target and their density. The stopping length of the ^{1}H in one bar of ^{3}He and N$_2$ is 5.1 cm and 1.0 cm respectively, and for the ^{3}H the stopping length is 1.9 cm and 0.3 cm in one bar of ^{3}He and N$_2$ respectively. The total stopping length values L$_1$ for the ^{1}H and L$_3$ for the ^{3}H for the for cells used in this work are given in Table 1. As can be seen the size of our cells is comparable to these stopping lengths, with some values larger than the cell size and others much smaller, thus the captured power will be varying significantly over our range of cells.

The amount of captured power density, i.e. average energy per second per unit volume captured in the gas by the slowing of the charged particles created by the ^{3}He-neutron capture reaction, was therefore estimated with a simple model. The random paths of the 573 keV ^{1}H, and 191 keV ^{3}H created when a neutron is absorbed by a ^{3}He nucleus are simulated. Then given the location in the cell where they originated we calculate whether or not the particles are stopped in the gas or by the cell's wall. The particles stopped in the gas are then used to calculate the average captured power density, and the particles reaching the wall are considered to deposit their energy there. We do this because the energy deposited along the particles path is a function of particle velocity, with more energy deposited per unit length as the particle becomes slower near the end of the particle's range. Therefore since for the purposes of this discussion, where we discuss our measurements of alkali-metal relaxation measured along a line through the center of the cell, we feel this crude model is sufficient to discuss the data.

As can be seen in Fig. 4B the fast component is relatively constant over the range of captured power densities. When scaled by the square root of absorbed neutron flux the 0 N$_2$ cell fillings (i.e. the 0.4 bar and 1.4 bar ^{3}He points) show nearly the same increase in alkali-metal relaxation despite the different captured power densities. For the other cells it could be argued that the slow component is increasing with captured power density. Given the caveats of the valved
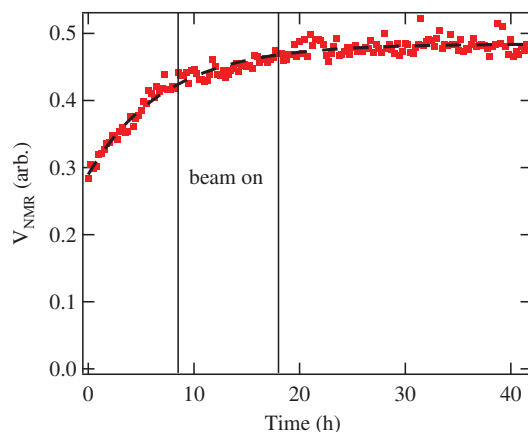
Figure 5. The measured relative ^{3}He polarization vs. time for the Roadrunner cell, a double chamber cell, via NMR free induction decay. During the time labelled "beam on" the spin filter portion of the cell was exposed to the flux of the neutron beam while continuing to polarize the cell via the spin-exchange chamber which was outside of the neutron beam. The observed ^{3}He polarization was not affected by the absorbed neutron flux in the spin filter chamber.

cell data, namely the unknown influence of the cell impurities, it is hard to draw a conclusion whether [N$_2$] or the captured power density is the only relevant or more important parameter from the data in Figs. 4A and 4B alone.

3. Double chambered cell

Provided the ionization effects do not cause direct mechanisms leading to nuclear spin relaxation of the ^{3}He, then a clear solution would be to use double chambered cells where the optical pumping process is isolated from the neutron absorption region. In the double chamber cell we used here, called the Roadrunner cell, the two chambers of approximately equal volumes of 30 cm^3 are connected by a small 6 mm inner diameter 5 cm long transfer tube to allow for transport of polarized ^{3}He between the chambers. As a test of this principle we installed the Roadrunner cell and polarized the spin-exchange chamber in situ while exposing the neutron spin filter chamber to the high neutron flux. The relative ^{3}He polarization was monitored using NMR free induction decay. Fig. 5 shows that the trend in the ^{3}He polarization was not modified by the neutron absorption. After this test we removed the cell and calibrated the remaining ^{3}He polarization on a different beam line were it was found to have reached over 50% during this test. Full details of this test have been described in Ref. [12].

4. Comparison to prior work and conclusions

The work conducted in the PF1B experiments, Ref. [12], measured the additional alkali-metal relaxation as a function of incident neutron flux and found a square root dependence on the absorbed flux for a given cell. This square root dependence was measured using sealed cells by varying the incident flux using calibrated neutron absorbers, keeping other parameters and experimental conditions fixed and thus was a robust measurement. Most of the cells in this work had similar levels of neutron absorption and also had similar values of [N$_2$], ranging from 0.07 bar to 0.12 bar, except for one cell which had 0.5 bar N$_2$. The cell with 0.5 bar N$_2$ clearly showed a much higher level of neutron induced alkali-metal relaxation. This indicates at least two dependent parameters to consider when comparing the two experiments.
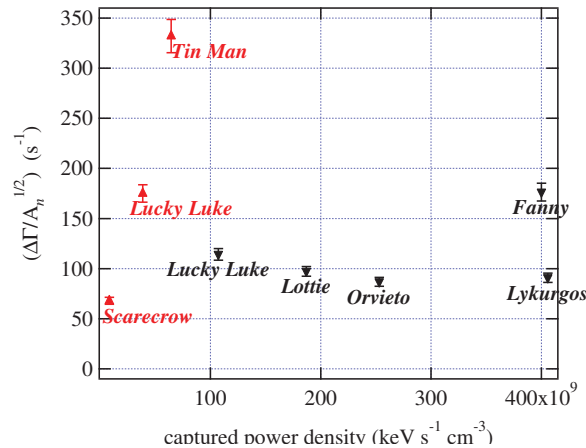
Figure 6. The measured change in alkali-metal relaxation verses captured power density for the cells from the PB1B experiment [12] (black downward triangles) and the sealed cells from this work (red upward triangle). All of the values of $\Delta\Gamma$ have been normalized to the square root of the normalized absorbed neutron flux, where the normal neutron flux (i.e. flux=1) was taken as the full flux of the tomography beam line used in this work.

The data for the Lucky Luke cell from this experiment can be compared with its data from the PF1B experiment because it was measured in both beams. When the values for the Lucky Luke cell from the PF1B data are fit to the square root of absorbed neutron flux, the fit values would predict a measured increase in alkali-metal relaxation of 67 s^{-1} for the measured neutron flux of the tomography beam line and ^{3}He density of the Lucky Luke cell. We measured 100 s$^{-1} \pm 5\%$ and feel this is reasonable agreement given the different conditions of the two experiments. We can surmise the limited knowledge of the spectrum of the tomography beam used here, or some other factor such as perhaps sampling a different location in the cell with our probe beam could lead to such a difference.

In Fig. 6 we plot the data from the the sealed cells in this work and the data from PF1B for $\Delta\Gamma/A_n^{1/2}$ versus captured power density. To account for the differences in absorbed neutron flux from the two beams we have used the measured neutron flux of the tomography beam in this work as a normalization constant. The relative neutron absorptions of the cells used in the PF1B experiment, for the energy spectrum of that beam, were given in Ref. [12], then given the flux on PF1B was 4.7/2.4 or 1.96 times that of the tomography beam, one can normalize the PF1B data to the square root of the absorbed neutron flux relative to the flux of the tomography beam. In this plot we can see the data from the PF1B experiment did not show a dependence on the captured power density, the only indication was of a dependence of the effect on [N$_2$]. The magnitude of the neutron induced relaxation observed here, is slightly higher, after scaling to the square root of absorbed neutron flux as stated above, but within reason given differences in the two experiments.

In conclusion, it is still not possible to determine the definitive origin of the mechanism involved in the unexpectedly high alkali-metal relaxation observed in high flux neutron beams. The measurement of the square root dependence was not repeated during this study but is assumed from the prior work and used to compare the data obtained in this work. We have confirmed that the neutron induced alkali-metal relaxation is increasing with [N$_2$] but it is unclear if this is due to a relaxation mechanism involving the nitrogen directly, or because of the effect of nitrogen density on the charged particle stopping power of the cell; the data from the

PF1B work and the valved cell data in this work may lead one to different conclusions. We have confirmed the presence of two time scales for neutron induced alkali-metal relaxation. The fast component happens on a time scale of less than 1 s and seems relatively constant with respect to [N$_2$] or captured power density. The slow component is increasing strongly with respect to captured power density or [N$_2$].

It is hard to imagine a way to eliminate this effect given the fast component alone such that efficient optical pumping could be done under conditions of absorption of extremely high neutron flux. At moderate flux levels the effect could likely be overcome with higher power optical pumping sources. Whereas at the highest neutron flux we believe the practical solution will be to perform the polarization of the ^{3}He outside of the neutron beam. With SEOP this can be accomplished in an in situ polarizer using a double chambered cell following the success using this technique for polarized electron scattering targets [18].

5. Acknowledgments

References

  [1] Andersen K H, Jullien D, Petoukhov A K, Mouveau P, Bordenave F, Thomas F and Babcock E 2009 *Physica B-Condensed Matter* **404** 2652 – 2654
  [2] Chen W C, Erwin R, McIver-III J W, Watson S, Fu C B, Gentile T R, Borchers J A, Lynn J W and Jones G L 2009 *Physica B-Condensed matter* **404** 2663–2666
  [3] Nacher P J and Leduc M 1985 *Jounal de Physique* **46** 2057–2073
  [4] Chann B, Babcock E, Anderson L W, Walker T G, Chen W C, Smith T B, Thompson A K and Gentile T R 2003 *J. of Appl. Phys.* **94** 6908–6914
  [5] Babcock E, Chann B, Nelson I A and Walker T G 2005 *App. Optics* **44** 3098–3104
  [6] Babcock E, Nelson I A, Kadlecek S, Driehuys B, Anderson L W, Hersman F W and Walker T G 2003 *Phys. Rev. Lett.* **91** 123003
  [7] Chen W C, Gentile T R, Walker T G and Babcock E 2007 *Phys. Rev. A* **75** 013416
  [8] Chen W C, Armstrong G, Chen Y, Collett B, Erwin R, Gentile T R, Jones G L, Lynn J W, McKenney S and Steinberg J E 2007 *Physica B Condensed Matter* **397** 168–171
  [9] Babcock E, Mattauch S and Ioffe A 2011 *Nuclear Instruments and Methods A* **625** 43 – 46
 [10] Chen W C, Gentile T R, Fu C B, Watson S, Jones G L, McIver J W and Rich D R 2011 *submitted to IOP journal of physics conference series, this issue*
 [11] Abele H, Dubbers D, Hase H, Klein M, Knopfler A, Kreuz M, Lauer T, Markisch B, Mund D, Nesvizhevsky V, Petoukhov A, Schmidt C, Schumann M and Soldner T 2006 *Nuclear Instruments and Methods A* **562** 407–417
 [12] Babcock E, Boag S, Becker M, Chen W C, Chupp T E, Gentile T R, Jones G L, Petukhov A K, Soldner T and Walker T G 2009 *Phys. Rev. A* **80** 033414
 [13] Bonin K D, Walker T G and Happer W 1988 *Phys. Rev. A* **37** 3270–3282
 [14] Coulter K P, McDonald A B, Cates G D and Happer W 1989 *Nuclear Instruments and Methods A* **276** 29–34
 [15] Babcock E, Boag S, Andersen K H, Becker M, Beechamb C, Bordenave F, Chastagnier J, Chen W C, Chung R, Chupp T E, Elmore S, Fouilloux P, Gentile T R, Jullien D, Lelievre-Berna E, Mouveau P, Petoukhov A, Revert M and Soldner T 2009 *Physica B-Condensed Matter* **404** 2655–2658
 [16] Franzen W 1959 *Physical Review* **115** 850–859
 [17] Wagshul M E and Chupp T E 1994 *Phys. Rev. A* **49** 3854–3869
 [18] Singh J, Dolph P, Mooney K, Nelyubin V, Tobias A, Kelleher A, Averettt T and Cates G 2009 *SPIN PHYSICS Book Series: AIP Conference Proceedings* **1149** 823–828